Inorganic Chemistry Communications 154 (2023) 110952

Contents lists available at ScienceDirect

Inorganic Chemistry Communications

journal homepage: www.elsevier.com/locate/inoche

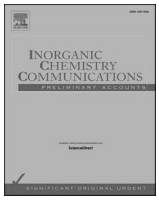

Short communication

Structural, magnetic, antimicrobial and hemolysis properties of sol–gel derived iron manganese tri oxide ($FeMnO_3$) nanostructures

C. Vinoth [a], J. Ramana Ramya [b,*], J. Gajendiran [a,*], S. Gnanam [c,*], S. Gokul Raj [d], G. Ramesh Kumar [e], M. Karthikeyan [a]

[a] Department of Physics, Vel Tech Rangarajan Dr. Sagunthala R&D Institute of Science and Technology, Avadi, Chennai 600 062, India
[b] Department of Periodontics, Saveetha Dental College and Hospitals, Saveetha Institute of Medical and Technical Sciences (SIMATS), Chennai 600077, India
[c] Department of Physics, School of Basic Sciences, Vels Institute of Science, Technology & Advanced Studies (VISTAS), Pallavaram, Chennai-600 117, India
[d] Department of Physics, C. Kandaswami Naidu College for Men, Annanagar, Chennai 600102, India
[e] Department of Science and Humanities, University College of Engineering Arni, Anna University Chennai, Thatchur, Arni 632 326, India

ARTICLE INFO

Keywords:
Nanostructures
Structural studies, Magnetism properties
Antibacterial activity
Hemolysis assay

ABSTRACT

Nanocrystalline Iron Manganese Tri Oxide ($FeMnO_3$, abbreviation name IMTO) material was attempted via colloidal solution followed by gel formation and subsequent processing at a calcined temperature of 480 °C. The above-mentioned compound was investigated for its structural characteristics, magnetic behavior, antibacterial response, and hemolysis experiment for spintronics and biomedical applications. The cubic crystal structure and weak ferromagnetic behaviour were noticed for the synthesized material from the powder X-ray diffraction (XRD) pattern and Vibrating Sample Magnetometer (VSM) studies. The surface structure of the title compound is noticed in aggregated spherical particles using Scanning Electron Microscopy (SEM) analysis. The antimicrobial activity of IMTO samples against gram-positive strains such as Streptococcus mutans (S. mutans) and Staphylococcus aureus (S. aureus) and gram-negative strains like Escherichia coli (E. coli) and Pseudomonas aeruginosa (P. aeruginosa) has been performed, followed by measurements of the zone of inhibition and their values are elucidated in detail. The hemolysis assay was carried out by taking human blood with the synthesized compound at various concentrations (5, 10, and 15 mg/mL), and the results showed its biocompatible nature.

1. Introduction

Very limited literature reports are available on the development of $FeMnO_3$ (IMTO)-based compounds using various chemical synthesis routes, followed by tests on Li-ion batteries, supercapacitors, energy storage devices, electro-optics devices, waste water treatment, and biomedical applications, etc. [1–18]. Further, excellent retention and cycling stability, high capacity characteristics, good dielectric properties, antiferromagnetic behaviour, good catalytic and antibacterial performance, and so on can be found in the aforementioned literature.

Various top-down approaches, such as precipitation, solvothermal, chemical oxidative, chemical solution deposition, green synthesis, pyrolysis, sol–gel, hydrothermal, self template, combustion, non-ionic surfactant assisted electrospun, mechanochemical, sol–gel auto combustion, mechanical alloying and solid state reaction methods are used to make the IMTO-based compound [1–22]. The above-mentioned methods have some demerits, like the synthesis step's prolonged reaction time interval processing at high temperatures autoclave deposition steps and the chemical oxidative process.

The current work focuses on the study of the structural and surface characteristics, magnetic properties, and biological activity (antibacterial and hemolysis) of synthesized IMTO nanostructures via the sol–gel route. The VSM study revealed that the synthesized compound has weak ferromagnetic behaviour at room temperature. Antibacterial activity of synthesized IMTO nanostructures against the four bacterial strains (S. mutans, S. aureus, E. coli, and P. aeruginosa) is chosen in the experiments followed by their zone of inhibition values and response in microbial activity results, which are elaborated in detail for the first time. In addition, the synthesized compound is biocompatible nature confirmed by the hemocompatibility test.

2. Experimental

The following chemicals, such as iron (III) nitrate hydrate (Fe

* Corresponding authors.
E-mail addresses: ramyavthu@gmail.com (J. Ramana Ramya), gaja.nanotech@gmail.com (J. Gajendiran), gnanam.nanoscience@gmail.com (S. Gnanam).

https://doi.org/10.1016/j.inoche.2023.110952
Received 11 April 2023; Received in revised form 4 June 2023; Accepted 16 June 2023
Available online 17 June 2023

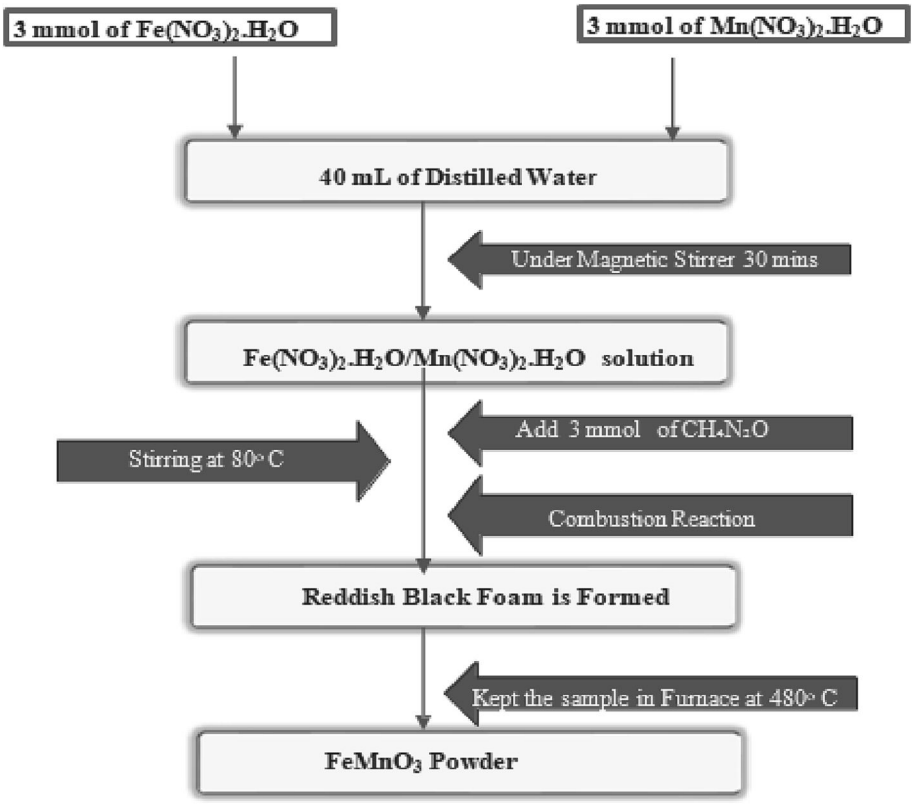

Fig. 1. Flow chart of the IMTO material.

Table 1
Instrument details of the synthesized compound.

S. No	Characterization	Instrument name
1	X-Ray Diffraction	X'Pert PRO Powder XRD Instrument
2	SEM/EDX	JEOLJSM −67001.SEM
3	Vibrating Sample Magnetometer (VSM)	Lakeshore VSM Model 740

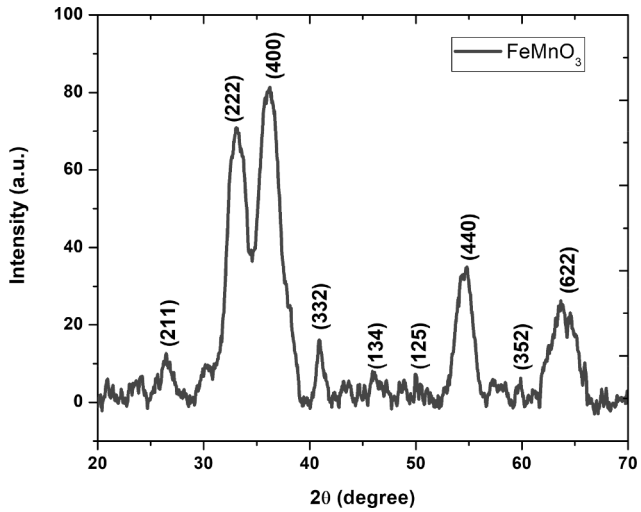

Fig. 2. XRD pattern of the synthesized IMTO powder.

$(NO_3)_2{\cdot}H_2O$) (Aldrich, purity 99.9%), manganese (II) nitrate hydrate ($Mn(NO_3)_2{\cdot}2H_2O$) (Aldrich, purity 99.9%), urea (CH_4N_2O) (Aldrich, purity 99.9%), and distilled water, were used to synthesize the title compound.

In a typical synthesis, 3 mmol of $Fe(NO_3)_2{\cdot}H_2O$ and $Mn(NO_3)_2{\cdot}2H_2O$ were dissolved in 40 ml of distilled water for 30 min with magnetic stirring. Further, 3 mmol of CH_4N_2O was added to the above mixture while magnetic stirring at 80 °C, resulting in the formation of reddish-black foam during the combustion reaction. Finally, the $FeMnO_3$ powder was formed when the sample was kept in a furnace at 480 °C. The chemical synthesis reaction step-through flow chart is shown in Fig. 1. The synthesized IMTO materials were characterized by powder XRD, SEM, EDX, VSM, antibacterial, and hemolysis analysis. The above-mentioned characterization instrument details are given in Table.1.

3. Results and discussion

The XRD pattern of the title compound powder was scanned between the ranges of 20° and 70° by means of powder XRD analysis and is shown in Fig. 2. The two sharp diffraction intensity peaks were noticed at $2\theta = 33.11°$ and 36.27°, which correspond to the miller index planes of (222) and (400), respectively [12]. Furthermore, 2θ values at 26.4°, 40.90°, 46.10°, 49.95°, 54.67°, 59.87°, and 63.67°, which correspond to planes indexed in the XRD pattern as (211), (332), (134), (125), (440), (352), and (622). The obtained XRD pattern of the synthesized material was compared to the reported XRD pattern of the IMTO material [2], which authenticated the cubic crystal structure (ICSD.No 33561) [2]. The average crystallite size of the IMTO compound is computed to be 50 nm from the observed strong diffraction intensity peaks at 38°, using the Debye Scherer formula ($D = K\lambda/\beta\cos\theta$, where d is the average crystallite size (nm), K is a constant usually equal to 0.89, λ is wavelength of X-rays (1.54 Å), β is the full-width half maximum (FWHM), θ is the diffraction angle) [23].

Using the SEM analysis, the title compounds are scanned and

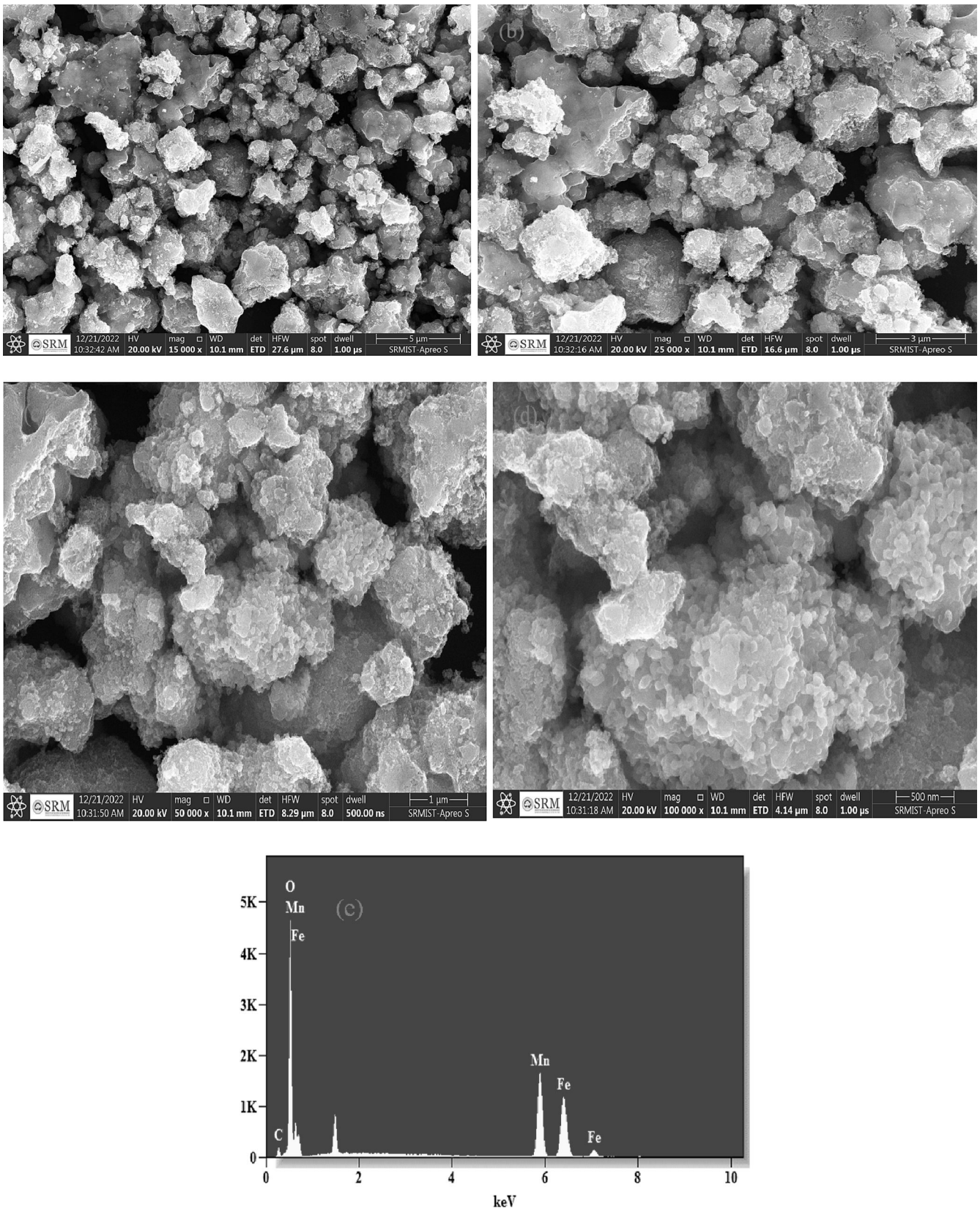

Fig. 3. Different magnification microstructure pictures of IMTO (a) 5 μm, (b) 3 μm, (c) 1 μm, 9d) 500 nm and (e) EDX spectrum of the iron managnese oxide.

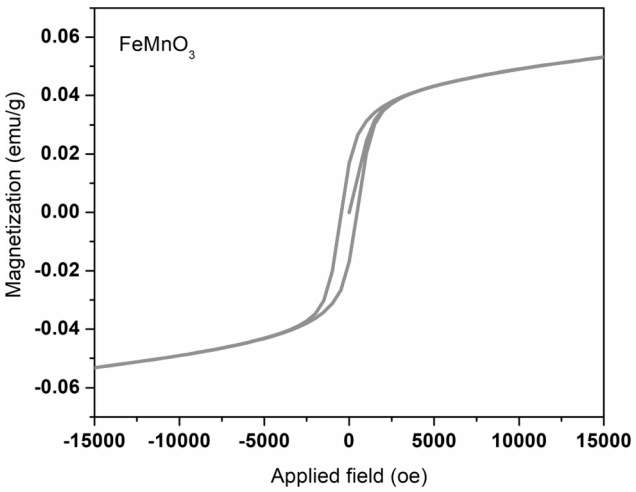

Fig. 4. M−H curve of the IMTO powder.

recorded in different magnification images of the surface morphologies and structures of the synthesized IMTO material, as shown in Fig. 3 (a-d). The microstructure of IMTO reveals that aggregated spherical particles formed. Fe, Mn, and O are traced from the EDX spectrum (Fig. 3e). The presence of a carbon peak is caused by the grid. It is evident from the above EDX results that the synthesized material is iron manganese oxide.

The magnetic properties of the title compound were tested through the VSM analysis. A tiny hysteresis loop (Fig. 4) was noticed in the VSM study, which represented that the title compound has weak ferromagnetic behaviour [18]. The other results, the magnetic saturation, coercive force, and residual magnetism values, are detected to be 0.05 emu/g, 465.63 Oe, and 16 $\times$ 10^{-3} emu/g, respectively, from the magnetization vs. applied magnetic field (M−H) curve. The low magnetic saturation might be due to an interaction alignment of Fe and Mn with respect to the applied magnetic field. The above-mentioned characteristics would be very useful in spin driven based devices. Some researchers investigated the magnetic properties of IMTO materials by different chemical routes [18–22]. They found moderate coercivity values for IMTO. The synthesized material has obtained coercivity values comparable with the reported coercivity values of IMTO materials [18–22].

In Table 2, the magnetic properties of the synthesized compound are compared to the reported magnetic properties of $FeMnO_3$ material. According to Table 2, the magnetic behaviour of the $FeMnO_3$ material changed depending on the chemical synthesis methods. When compared to the reported coercivity value of $FeMnO_3$, the synthesized material has obtained relatively higher coercivity values.

The antimicrobial activity of IMTO samples against the gram-positive and gram-negative bacterial strains was estimated, and the zone of inhibition was shown in Fig. 5. Throughout the experiments, amoxicillin (an antibiotic) is used as the positive control and distilled water is used as the negative control. In the experiments, gram-positive strains such as S. mutans and S. aureus and gram-negative strains like E. coli and P. aeruginosa were chosen. The diameter of the zone of inhibition of the IMTO against different bacterial strains is summarized in Table 3. The positive control showed 27 $\pm$ 1 and 25 $\pm$ 1 mm for the S. mutans and S. aureus, respectively. The IMTO sample showed the diameter of the zone of inhibition was observed to be 16 $\pm$ 2 for S. mutans and 15 $\pm$ 1 mm for S. aureus. The negative control showed no zone of inhibition. The diameter of zone of inhibition of the positive control against E. coli and P. aeruginosa showed 28 $\pm$ 1 and 30 $\pm$ 1 mm whereas, the IMTO sample showed 18 $\pm$ 2 mm and 20 $\pm$ 1 mm, respectively.

The gram-positive strains have a thick peptidoglycan cell wall thickness of 20 to 30 nm, and the cell walls of gram-negative strains are made up of a very thin peptidoglycan membrane and the lipid bilayer membrane of 3 nm. The thick peptidoglycan membrane of gram-positive strains makes them resistant to antibiotics and nanomaterials when compared to the gram-negative strains. Further, Vasiljevic et al. [15] reported that IMTO exhibited negative zeta potential, and the negative surface of the IMTO attracts the positively charged bacterium by electrostatic attraction. As a result, the nanoparticles penetrate and enter the thick peptidoglycan membrane of the gram-positive bacteria. The metal oxide nanoparticle produces reactive oxygen species (ROS) inside the pathogen's cell, leading to the production of dioxygen. Since the particle size of the IMTO is around 50 nm, there would be a large amount of dissolved iron, which is responsible for the inhibitory effect of the bacterial strains [15]. The dissolved iron leaches the pathogen's cell wall from the negatively charged iron and disrupts the internal components of the bacteria, resulting in DNA damage and protein denaturation and eventually killing the pathogens. A schematic diagram of the antibacterial mechanism of the synthesized IMTO is presented in Fig. 5e.

The compatibility of RBCs is an important phenomenon for nanomaterials to serve as a potential biological carrier. The hemocompatibility assay of IMTO (Fig. 6) showed high hemocompatibility at low concentrations (5 mg/mL). When the concentration was increased to 10 mg/mL and 15 mg/mL, the sample showed a moderate percentage of erythrocyte lysis. The sample is biocompatible since it exhibited a percentage of hemolysis within the permissible limits of the ASTM standards. The Fe^{2+} ions in the IMTO could be the reason for the rupture of erythrocytes caused by the higher concentrations [24]. Even though the blood toxicity of IMTO was appreciable, the incorporation of iron oxide showed splendid interactions on and inside the RBCs, which resulted in a change in the hemolytic percentage.

4. Conclusion

In this work, sol–gel synthesis-assisted IMTO nanostructures were fabricated, followed by investigations into their crystalline structure, surface image characterization, magnetism features, and antibacterial activity. The synthesized IMTO powder was analyzed using powder XRD, and its observed diffraction peaks resulted from the XRD pattern, which confirmed the arrangement of the cubic crystal system. With the help of high- intensity diffraction peaks from the XRD, the crystallite size

Table 2
Comparison of the reported magnetic properties of $FeMnO_3$ material with the present work.

Material	Synthesis method	Magnetic saturation (emu/g)	Coercivity (Oe)	Retentivity (M_r) (emu/g)	Magnetism behaviour	References
$FeMnO_3$	Mechano- synthesis	–	–	–	Ferrimagnetic	Rayaprol et al [18]
$FeMnO_3$	Sol-gel auto combustion	0.348	405	–	Antiferromagnetic	Gowreesan et al. [19]
$FeMnO_3$	Mechanical alloying	–	–	–	Ferrimagnetic	Seifu et al. [20]
$FeMnO_3$	Mechanochemical synthesis	–	200	–	Ferrimagnetic	Rayaprol et al [21]
$FeMnO_3$	Solid-state reaction	–	299	0.296	Ferrimagnetic	Asep Ridwan Nugraha et al [22]
$FeMnO_3$	Sol-gel	0.05	465.63	0.016	Ferromagnetic	In this present work

Note
here, - means not discussed the particular magnetic parameter.

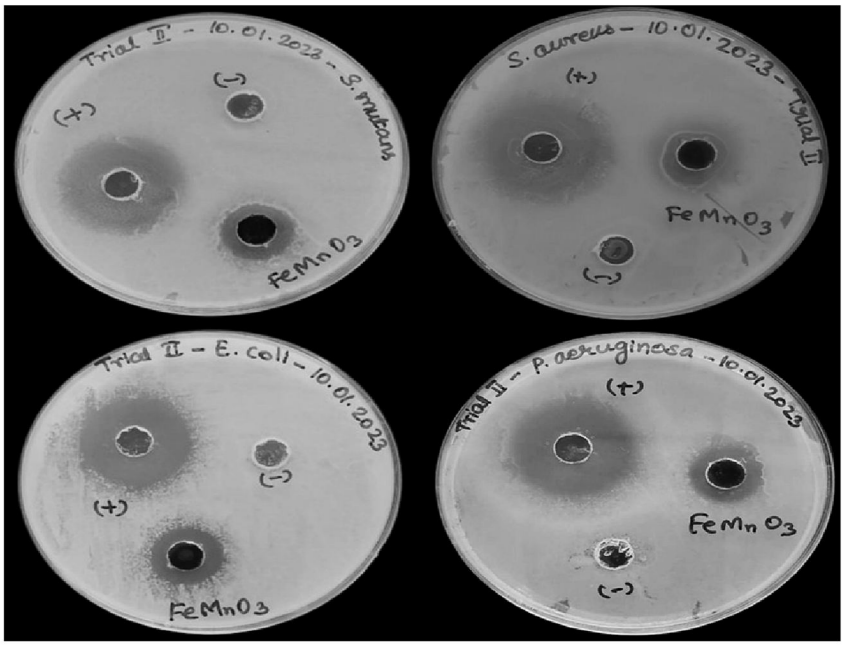

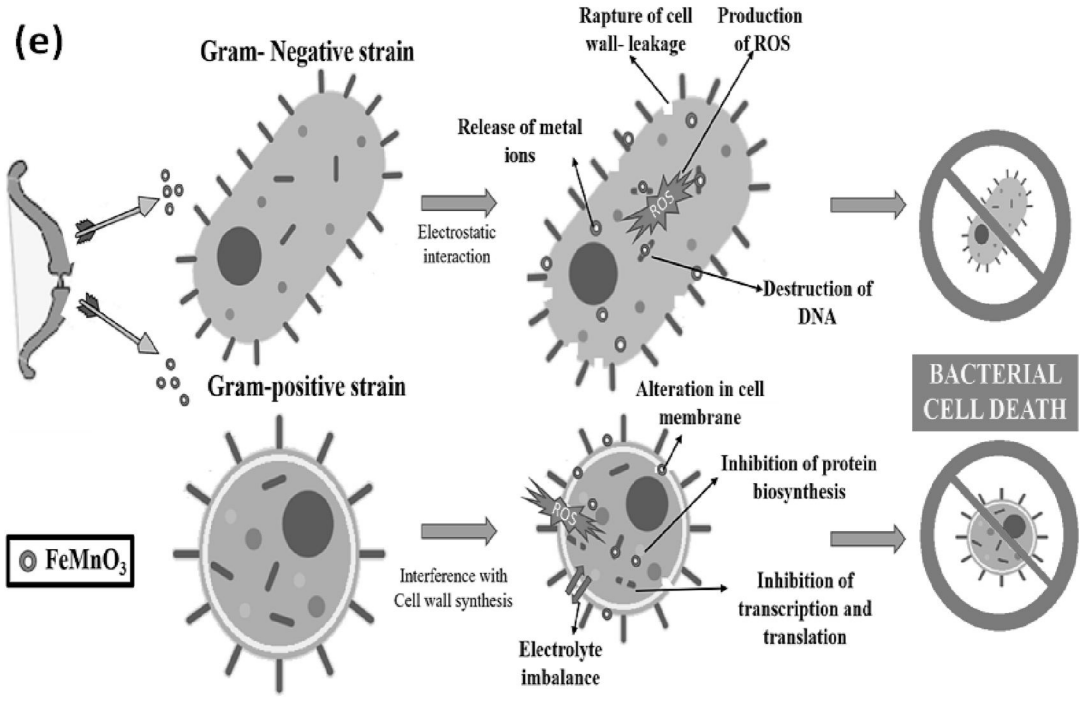

Fig. 5. Antimicrobial activity of IMTO against (a) Streptococcus mutans, (b) Staphylococcus aureus, (c) Escherichia coli, and (d) Pseudomonas aeruginosa, (e) Schematic diagram of antibacterial mechanism of the synthesized IMTO nanostructures.

Table 3
The diameter of zone of inhibition of the IMTO against different bacterial strains.

S. No	Bacterial Strain	Diameter of zone of Inhibition in mm		
		Positive control	Negative control	IMTO
1.	S. mutans	27 ± 1	0	16 ± 2
2.	S. aureus	25 ± 1	0	15 ± 1
3.	E. coli	28 ± 1	0	18 ± 2
4.	P. aeruginosa	30 ± 1	0	20 ± 1

of the synthesized compound was computed to be 50 nm. The synthesized title compounds showed aggregated spherical particles throughout the surface, which was confirmed by the SEM analysis. Only synthetic compound elements were traced in the EDX spectrum. A soft ferromagnetic characteristic was noticed in the above-mentioned compound from the VSM study, and its results would be very useful in spin-driven device applications. In the antibacterial experiments, gram-positive strains such as S. mutans and S. aureus and gram-negative strains like E. coli and P. aeruginosa were selected. Among the bacterial strains, IMTO against P. aeruginosa has found a relatively higher antibacterial response compared to S. mutans, S. aureus, and E. coli. In addition, all

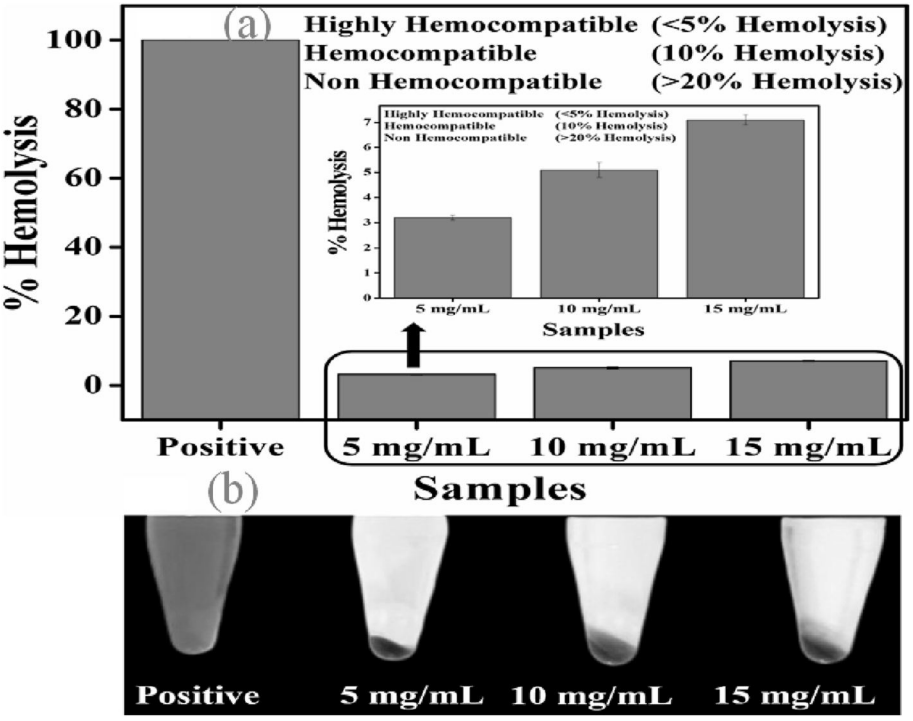

Fig. 6. Hemocompatibility of IMTO a) Histogram of percentage of hemolysis and b) Microcentrifuge tubes of positive control, 5 mg/mL, 10 mg/mL, and 15 mg/mL displaying the photographic images of material treated with IMTO.

bacterial strains respond well to microbial activity. The percentage of hemolysis for the samples was collected, and the obtained hemolysis values were compared with the ASTM standards. Hemolysis experiments showed the synthesized IMTO to be hemocompatible. Based on the magnetic studies, antibacterial activity, and hemolysis experiment results, the synthesized IMTO is suitable for biomedical applications.

CRediT authorship contribution statement

C. Vinoth: Methodology, Investigation. **J. Ramana Ramya:** Writing – review & editing. **J. Gajendiran:** Investigation, Conceptualization, Writing – review & editing. **S. Gnanam:** Conceptualization, Writing – review & editing. **S. Gokul Raj:** Writing – review & editing. **G. Ramesh Kumar:** Writing – review & editing. **M. Karthikeyan:** Formal analysis.

Declaration of Competing Interest

The authors declare that they have no known competing financial interests or personal relationships that could have appeared to influence the work reported in this paper.

Data availability

Data will be made available on request.

References

[1] J. Yao, J. Wu, Y. Yang, S. Xiao, Y. Li, J. Alloys. Compd. 848 (2020) 156444.
[2] H. Wei, Y. Guo, C. Gao, Z. Wang, Advanced, Powder Technol. 32 (2021) 4322–4329.
[3] Anum Jameel, Muhammad Munir Sajid, Amir Muhammad Afzal, , Asmat Ullah, et al. Journal of Electronic Materials.51 (2022) 900-909.
[4] Q. UlAin, S. Ali, S. Jamil, S. Bibi, S.R. Khan, S.U. Rehman, et al., Mater. Sci. Semicond. Process. 144 (2022) 106630.
[5] Y.u. Zhang, J. Li, X. Chen, W.u. Shuxiang, N.i. Qin, D. Bao, Thin Solid Films. 754 (2022) 139320.
[6] Abhikha Sherlin V, Xavier Benadict Joseph, Sea-Fue Wang, Jeena N. Baby, Mary George, J. Mole. Liq. (2022) 120421.
[7] Y. Xu, S. Xiang, X. Zhang, H. Zhou, H. Zhang, J. Hazard. Mater. 439 (2022) 129575.
[8] W. Wang, P. Zhang, S. Li, C. Zhou, S. Guo, J. Liu, et al., J. Power Sources. 475 (2020) 228683.
[9] J.-Q. Li, F.-C. Zhou, Y.-H. Sun, J.-M. Nan, J. Alloys. Comp. 740 (2018) 346–354.
[10] M. Li, W. Xu, W. Wang, Y. Liu, B. Cui, X. Guo, J. Power Sources. 248 (2014) 465–473.
[11] X. Hou, G. Zhu, X. Niu, Z. Dai, Z. Yin, Q. Dong, et al., J. Alloys Compd. 729 (2017) 518–525.
[12] L.S. Lobo, A. Rubankumar, Ionics. 25 (2019) 1341–1350.
[13] B. Saravanakumar, S.P. Ramachandran, G. Ravi, V. Ganesh, Ramesh K Guduru, R Yuvakkumar, Mater. Res. Express 5 (2018) 015504.
[14] M. Chi, S. Chen, M. Zhong, C. Wang, X. Lu, Chem. Commun. 54 (2018) 5827–5830.
[15] Z.Z. Vasiljevic, M.P. Dojcinovic, J.B. Krstic, V. Ribic, N.B. Tadic, et al., RSC Adv. 10 (2020) 13879–13888.
[16] Mohammad Hossein Habibi , Vala Mosavi, J. Mater Sci Mater Electron. 28(2017) 8473-8479.
[17] S. Xiao-Lu, S. Xiao-Fei, W.u. Liu Yan-Hua, C.-B. Yue, Z. Hong-Mei, Wuji Cailiao Xuebao. 34 (2019) 709–714.
[18] S. Rayaprol, S.D. Kaushik, Ceram. Int. 41 (2015) 9567–9571.
[19] S. Gowreesan , A. Ruban Kumar, App. Phy A .123 (2017) 689.
[20] D. Seifu, A. Kebede, F.W. Oliver, E. Homan, E. Hammond, C. Wynter, et al., J. Magn. Magn. Mater. 212 (2000) 178–182.
[21] S. Rayaprol, S.D. Kaushik, P.D. Babu, V. Siruguri, AIP Conference Proceedings. 1512 (2013) 1132.
[22] Asep Ridwan Nugraha, Ervin Nauval Arrasyid, Dedi, Agustinus Agung Nugroho, Mater. Sci. Forum. 1080 (2023) 139-145.
[23] J. Gajendiran, S. Gnanam, C. Parthasaradhi Reddy, G. Ramesh Kumar, V.C. Bharath Sabarish, S. Gokul Raj, K. Ramachandran, V.P. Senthil, V. Gopi, Inorg Chem. Commun. 135 (2022) 109101.
[24] M.A. Al-Akhras, K. Aljarrah, B. Albiss, A.A. Bala, I.O.P. Conf ser, Mater. Sci. Eng. 92 (2015) 012003.